New Instruments and Measuring Techniques

EXPERIMENTAL TECHNIQUES OF LOW-ENERGY ELECTRON DIFFRACTION

A. A. BABAD-ZAKHRYAPIN, N. S. GORBUNOV, and V. I. IZVEKOV

Usp. Fiz. Nauk 77, 727-748 (August, 1962)

INTRODUCTION

LOW-ENERGY electron diffraction is more complicated than the other diffraction methods—x-ray diffraction, standard (high-voltage) electron diffraction,* and neutron diffraction—with regard to both the experimental arrangements and the interpretation of data. The diffraction of low-energy electrons has therefore been used much less widely than x-ray diffraction or even high-voltage electron diffraction. Low-energy electrons have a much narrower range of usefulness than high-energy electrons; beams at energies of 10 to 10^3 eV can penetrate only a few atomic layers of matter. However, this very limitation makes low-energy electron diffraction necessary for investigating the structure of surface monolayers. Among the problems in this field are the structure of atomically clean crystal faces, the structure of chemisorbed gas layers, the kinetics of the initial stages of gas adsorption and metal oxidation etc. Other problems include the energy properties of atomically clean surfaces such as the inner potentials of crystals, work functions, the photoelectric effect, electron emission etc.

The development of low-energy electron diffraction, from the first experiments [2-4] to 1960, has been characterized by continual improvement of the apparatus and experimental techniques. Almost all data hitherto obtained by this method have been qualitative because no theory of slow-electron diffraction has been developed. In such diffraction low-speed electrons undergo predominantly dynamic scattering by matter. The description of this scattering must take into account the interaction between electrons and atomic fields as well as the interference of scattered waves in matter. The incompleteness of the theory lies in the fact that when these effects are taken into account no direct relationship is found between the symmetrical arrangement of atoms in matter and the observed extinctions. The fine structure of the diffraction maxima and the appearance of "forbidden" maxima have not been explained. Nevertheless, low-energy electron diffraction has enabled the observation of several new effects on solid surfaces, such as the ordered adsorption of gases on monocrystalline faces.

*Electron diffraction can be divided into three ranges of primary-beam energies: low-energy diffraction (<10^3 eV), the most highly developed and widely used standard electron diffraction method (<100 keV), and microdiffraction[1] (~400 keV).

The problems associated with low-energy electron diffraction are represented insufficiently in Soviet scientific literature. The only review of pre-war Soviet work is found in [5]. The present review will acquaint readers with the experimental techniques used in observing low-energy electron diffraction and indicates the fields in which this method can be used effectively.

1. EXPERIMENTAL TECHNIQUES USED TO OBSERVE LOW-ENERGY ELECTRON DIFFRACTION

A basic characteristic of the method is its high sensitivity to impurities; therefore in designing apparatus the removal of impurity sources is of paramount importance. This makes it necessary to use a vacuum of 10^{-9}—10^{-10} mm Hg, which is attained very simply since the diffraction tube has a small volume of 1—0.5 liter. The cleaning of samples in diffraction tubes requires special compartments for outgassing by heating and argon-ion bombardment.

1. Diffraction tubes. Diffraction tubes are usually made of Pyrex glass, which is easily cleaned and permits pressures of $\sim 10^{-10}$ mm Hg. Metal parts are made of nonmagnetic materials, most frequently of molybdenum. Figure 1 is a diagram of a diffraction tube.[6] The hot-cathode electron gun 1 produces an intense electron beam. The cathode of the gun is mounted off the axis of the crystal 6 (or 8) in order to prevent filament impurities from striking the crystal. The electron beam is guided into the tube by a grid imposing a deflecting electrostatic field.[7] In the space between the two cylinders 2 electrons can be either retarded or accelerated;[8] electron energy in the defined beam is thus regulated smoothly. The gap between the cylinders is sometimes surrounded by a ring in order to reduce the number of scattered electrons.[8] The beam becomes finally well-defined in the capillary collimator 3, and is then directed normally against the surface of the sample 6. Diffraction beams are registered by the electron collector 4. The vibrating-reed electrometer is connected to the inner box of the collector. The grounded middle box serves as a shield. The outer box is in electrical contact with the drum 5, around which the collector is rotated. The collector boxes are insulated from each other by mica sheets.

The electron current in the primary beam at the surface of a sample is usually $\sim 10^{-8}$ A; current con-

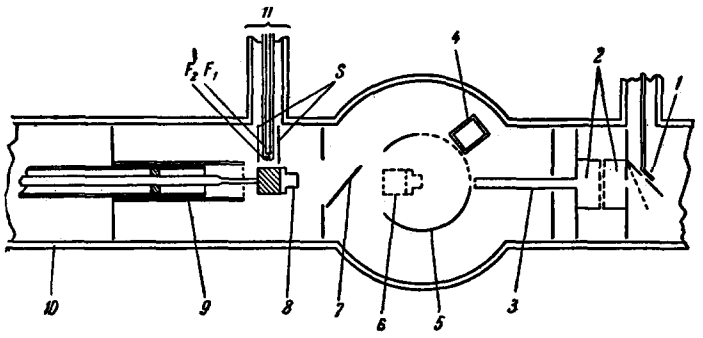

FIG. 1. Diffraction tube. 1 – filament of electron gun; 2 – cylinders controlling electron beam energy; 3 – collimator; 4 – electron collector; 5 – drum; 6 – crystal and crystal-holder in experimental position; 7 – door; 8 – crystal and crystal-holder in position for cleaning; 9 – glass shield; 10 – envelope; 11 – bombardment filaments.

stancy is maintained by a photocell arrangement controlling the heating current in the electron gun. Terrestrial magnetism is compensated by a Helmholtz coil 1 m in diameter (not shown in Fig. 1). The inner surface of the glass envelope is sometimes covered with a thin layer of deposited metal serving as an electrostatic shield. [9]

The diffraction chamber is separated from the cleaning chamber by the door 7, which keeps out impurities formed during the cleaning process. The crystal-holder has at least two degrees of freedom —translation along the tube axis and rotation around this axis. Translation along the axis is required to transfer samples from the cleaning chamber to the diffraction chamber; rotation is required for the investigation of diffraction effects in different azimuths. In the cleaning chamber samples are outgassed and are surface-cleaned by argon-ion bombardment. Electron bombardment produces heating during the outgassing process. Electrons are emitted by the spiral filament F_2. The crystal-holder is outgassed along with the sample.

A discharge in argon at 10^{-3} mm Hg produces ions for surface cleaning. A potential difference of 200—600 V is applied to the space between the door 7 and the surface of the sample at position 8. The electron beam produced by the filament F_1 (at the potential of the door) is accelerated by F_2, which thus functions as a positive grid. The cylinder S is negative with respect to the door and serves to limit the ionizing electron beam. A potential applied to the metal parts of the cleaning chamber shields them from argon-ion bombardment. During the ion cleaning the crystal-holder is enclosed in the glass shield 9; only the sample remains outside the shield. In the diffraction tube shown in Fig. 1 the primary electron beam is directed at normal incidence to the surface of the test crystal. It is thus difficult to register diffraction beams having directions close to the primary direction. Tubes of this type can register diffraction beams 10—15° from the normal to the crystal surface.

A diffraction tube without the foregoing shortcoming is described in [10]. An external magnetic field is used to permit the registration of diffraction beams close to the normal. The operation of this tube is described in Fig. 2. An electron beam from the gun P is accelerated

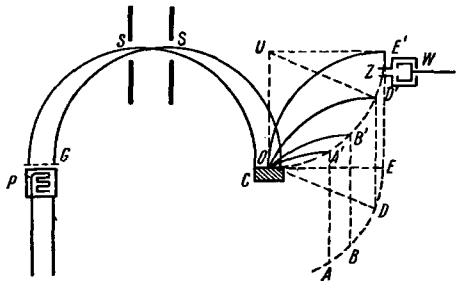

FIG. 2. Registration of magnetically deflected diffraction beams.

by the grid G. The magnetic field is perpendicular to the plane of the figure, so that the primary-beam trajectory is circular. The field strength is such that the beam passes through the slits SS and reaches the sample C at normal incidence. Diffraction beams will also have circular trajectories with the same radius as the primary beam.

Diffraction beams having different directions will be focused on the circle A'B'D'E' with its center at U; the centers of the trajectories will lie on the circle ABDE with its center at O. If the opening Z of the collector W remains horizontal while being moved along the circle A'B'D'E' the collector registers diffraction beams at practically all angles.

A diffraction tube employing this means of registering diffraction beams is sketched in Fig. 3. The glass tube is 8 cm in diameter and 90 cm long. The sample C is placed 12 cm from the electron gun P. The location of the slits SS limits the primary-beam trajectory to a 6-cm radius. The grid G made of Mo wire is part of the Mo chamber A; another Mo chamber is designated by the letter U. These chambers trap incoherently scattered (stray) electrons. The grid D captures electrons passing the sample C and also serves to measure the primary current in the absence of a sample. The crystal-holder and sample are fastened to the quartz tube Q, which is rotated and moved on the bearings BB by means of a magnet located outside the tube and by the crosspiece I. The crystal is grounded through the seal L. Outgassing and ion cleaning take place within the coil F. The linkage mechanism M maintains the horizontal position of the opening of the electron collector W.

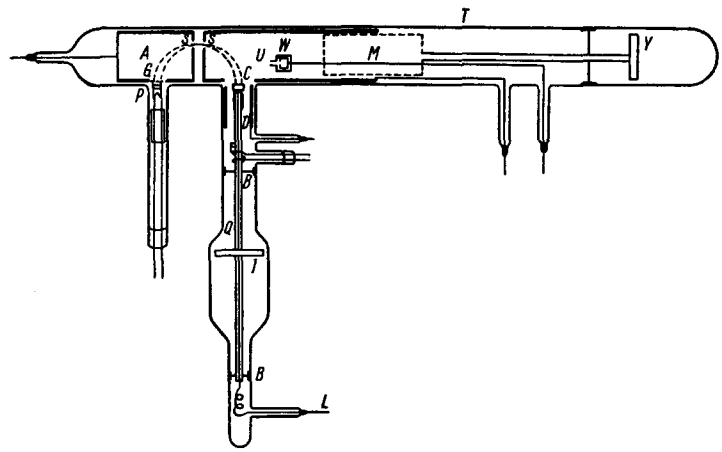

FIG. 3. Diffraction tube where diffraction beams are deflected magnetically.

The diffraction tube used in conjunction with a magnetic field permits reliable measurements of electron energy in the primary beam. This is extremely important in all electron diffraction investigations. In the measurement of low-speed electron energies we must consider the possibility of contact potential differences. In the case of 10—15-eV electrons such potentials can greatly change the wavelength λ calculated from the formula $\lambda = (150/V)^{1/2}$, where V is the accelerating potential.

The designer of the magnetic diffraction tube determined that in his apparatus the true accelerating potential was 7 V below that measured with a precision voltmeter. The difference between the true potential and the measured potential varied 2—3 V from day to day. These potential fluctuations are evidently associated with properties of the apparatus or of its constituent materials; it is noted in [11] that these fluctuations usually amount to a fraction of a volt.

2. Gas-handling systems. Before being admitted to the diffraction system argon is thoroughly purified in a special Mo-getter tube and is then fed into a fore volume for pressure reduction. Gas is admitted through a fine capillary leak with a mercury cutoff or through a high-vacuum valve, the former being used with mercury diffusion pumps and the latter with oil diffusion pumps.

Gas is also admitted to the diffraction tube for the study of adsorption through a fore volume where the pressure is reduced to 10^{-5} mm. The gas then passes into the diffusion pump, from which it diffuses into the diffraction tube.[12]

3. Vacuum system. The diffraction tube is evacuated by mechanical pumps to produce a fore vacuum and by diffusion pumps for the experimental vacuum. In early work[9] two glass mercury pumps and one oil pump were used in series, and vapor was removed from the system by liquid-air traps. Somewhat later[12] three-stage oil diffusion pumps were used with a liquid-air trap on each side.

In order to achieve a vacuum of 10^{-10} mm Hg the apparatus must first be outgassed. This is accomplished by repeated heating at 350° during continuous pumping, after which the pressure in the tube is reduced to $\sim 10^{-8}$ mm. Vaporization of a Mo getter improves the vacuum to 10^{-9}—10^{-10} mm.

More recently ion pumps have been used[13,14] to achieve 10^{-10} mm much more rapidly. The vacuum in diffraction tubes is measured with Bayard-Alpert manometers.[15]

4. Crystal-holder. A crystal-holder of the simplest construction is represented in Fig. 4.[6] The crystal is fastened to a Mo block that had previously been outgassed at a higher temperature than that used in outgassing the crystal. The surface of the block in contact with the crystal had been prepared carefully to prevent damage to the latter. The crystal is fastened to the block by either Mo springs (Fig. 4a) or Mo hooks (Fig. 4b). In the latter case nuts are used to apply the required pressure. This form of crystal-holder does not permit inclination of the crystal surface to the incident beam. Turning becomes possible when a more complicated crystal-holder is used.[16] In this case the crystal is adjusted within $\pm 0.5°$ by micrometer screws, using a goniometer and telescope.[9]

A special modification[12] of the crystal-holder represented in Fig. 4 enables the investigation of low-energy electron diffraction with regulated temperature of the sample.

5. Registration of diffraction patterns. Two methods are used to register diffraction patterns in diffraction tubes containing electron collectors. In one technique

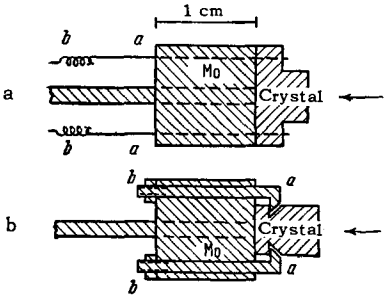

FIG. 4. Simplest crystal mountings. a) Crystal is pressed against Mo block by Mo wires a and springs b; b) Crystal is fastened to Mo block by hooks a and nuts b. Arrows indicate direction of primary electron beam.

the current in a fixed collector is measured as a function of the primary-beam energy, which is varied continuously by a precision potentiometer that is driven by the recorder chart drive. After each rotation of the potentiometer, i.e., after the required primary-electron energy interval has been studied, a solenoid-actuated mechanism moves the collector to the next position; this is usually done in 0.5° steps.

In the other technique diffraction patterns are registered by having the collector current measured as a function of the collector angle for different fixed primary-beam energies. In this case double-walled collectors with quartz insulation are used.

As already mentioned, low-energy electron diffraction is studied with normal incidence of the primary beam. This has a number of advantages over Bragg reflection at small-angle incidence. Diffraction beams can be registered in more than one azimuth, thus permitting the determination of atom positions in the surface layer at the same time that diffraction beams from deeper layers are also registered.

6. Diffraction tube with photographic registration. The design of this tube employs the principle of accelerating diffraction beams to energies sufficient for visible excitation of a fluorescent screen.[17] The electron beam from a thoriated tantalum cathode 1 is accelerated to 600 eV (Fig. 5).[14] A narrow beam is defined by a magnetic coil and the diaphragm 2. The beam is then slowed down to the required energy (by an arrangement not shown in Fig. 5) and is deflected from the central axis of the tube by the arrangement 3.

The well-defined beam impinges normally on the surface of the sample 6. Diffraction beams are accelerated to 1000—2000 eV by two grids 4 made of W wires 0.01 mm in diameter. The grids transmit 75% of the electrons reaching them. The grids are 2.5 mm apart, and the second grid is 5—10 mm from the fluorescent screen. The crystal is situated 44 mm from the first grid. The surface of the glass envelope 9 in the vicinity of the sample 6 is covered with a thin layer of tin oxide, which is at the same potential as the first grid (the second in order from the fluorescent screen) and the sample. Diffracted electrons thus move within a field-free space. The retarding field between the grids stops inelastically scattered electrons.

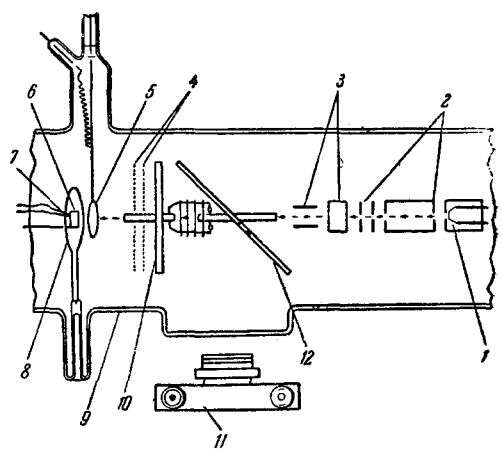

FIG. 5. Sketch of diffraction tube with photographic registration.

The diffraction pattern on the fluorescent screen 10 is observed by means of a mirror 12 positioned at 45° to the screen.

A flat W ribbon 8 surrounding the sample serves to heat the latter by electron bombardment and also to measure the vacuum during the sample-cleaning process.[18] The temperature of the crystal is monitored by the thermocouple 7. The grids and fluorescent screen are protected from contamination by the shield 5, which is moved by means of a magnet located outside the tube.

The retarding lens comprises two coaxial cylinders of equal diameters separated by a space containing a shielding coil. This diffraction tube permits a 1-μA primary beam 1 mm in diameter accelerated to 10 eV. The diffraction pattern on the fluorescent screen is photographed by the camera 11.

The above-described diffraction tube possesses only seeming advantages over tubes containing electron collectors. The registered portion of the diffraction pattern actually lies within an angle of 37° from the primary beam.[19] Some diffraction effects can therefore be overlooked. However, for a qualitative study of certain processes, such as the dynamics of gas adsorption, this type of chamber is entirely adequate. To determine the positions of atoms in the surface structure as many as 100 photographs at different primary energies are necessary.[19] The time required for this purpose is longer than the duration of the processes leading to the formation of the investigated structure. On the other hand, the simultaneous observation of the entire diffraction pattern gives more complete information concerning the surface structure than can be obtained by measuring diffraction beam currents. A serious shortcoming of the described tube is the design of the electron gun, where the fact that the thoriated cathode is in line with the sample permits possible thorium contamination of the investigated surface.

II. CHARACTERISTICS OF LOW-ENERGY ELECTRON DIFFRACTION

1. Diffraction effects. We shall now consider the conditions obtaining in the diffraction of low-energy electrons by a body-centered tungsten lattice ($a = 3.155$ Å).[20] Figure 6 shows a vertical section of this lattice perpendicular to the (112) plane. The arrangement of atoms in the azimuth AA′ is shown in Fig. 7 (2). With U and V denoting the direction of a primary beam having the wavelength λ, the diffraction of beams scattered by atoms Z and X at the angle Θ is subject to the condition

$$n_1\lambda = \sqrt{2}\, a \sin\Theta, \qquad (1)$$

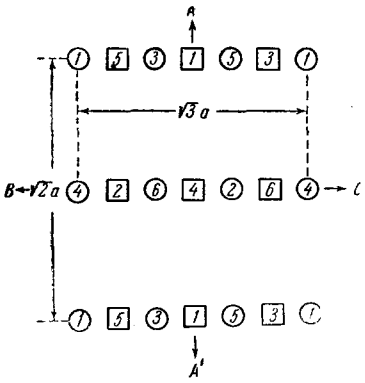

FIG. 6. Section through a body-centered cubic lattice perpendicular to the (112) plane. Circles designate atoms located at cubic vertices; squares designate atoms in body-centered positions.

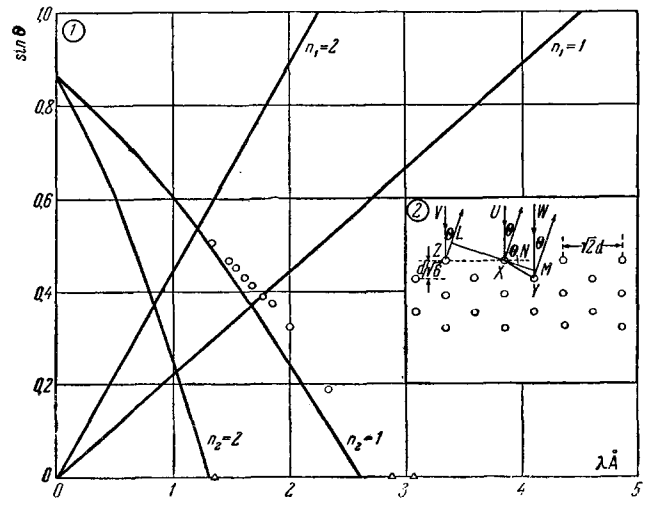

FIG. 7. Graphs of (1) the surface and volume conditions for $n_1 = 1,2$ and $n_2 = 1,2$, and (2) atomic structure represented by Fig. 6 in the AA′ azimuth. Experimental data are represented by open circles.

where n_1 is an integer (the order of diffraction). Constructive interference between beams diffracted from other layers is subject to the condition (Fig. 7)

$$NY + YM = n_2\lambda,$$

or

$$n_2\lambda = \frac{a}{\sqrt{6}} + 2\frac{a}{\sqrt{6}}\sin(30° - \Theta), \qquad (2)$$

where n_2 is also an integer. Both conditions, Eqs. (1) and (2), must be satisfied in the general case. Equation (1) is called the surface condition, while (2) is called the volume condition; both conditions are represented in Fig. 7 (1) for two values of n_1 and of n_2. The experimental data, which are represented by circles, are fitted very closely by the curve of the volume condition for $n_2 = 1$. The deviation from the theoretical curve results from the fact that refraction was not taken into account in the plots. As a result of refraction the wavelength in the crystal is λ', instead of λ, with the corresponding angle Θ'. The refractive index is given by

$$\mu = \frac{\lambda}{\lambda'} = \frac{\sin\Theta}{\sin\Theta'}. \qquad (3)$$

When refraction is taken into account (2) becomes

$$\lambda' = 1.29[1 + 2\sin(30° - \Theta)]. \qquad (4)$$

From (3) and (4) we obtain a formula for calculating the refractive index:

$$\mu = \frac{(\lambda/1.29)^2 + 2.685\lambda\sin\Theta + 4\sin^2\Theta}{2(\lambda/1.29 + 1.732\sin\Theta)}. \qquad (5)$$

Refraction can be neglected for diffraction beams in the direction $\Theta = 0$. In this case it is possible to determine directly the inner potential φ of the lattice from the difference between the actual potential at which the diffraction maximum is observed and the calculated potential.* Thus it was found in [20] that for a tungsten crystal in the azimuth AA′ (Fig. 6) we have $\varphi = 5.52$ V.

In connection with the volume condition (2) it must be remembered that low-energy electrons penetrate only two or three layers of atoms.

It was shown in [21] that a silver monolayer on the (100) face of a copper crystal produces a 70% reduction of diffraction intensity from copper at 300 eV. A silver monolayer on a (100) face of a gold crystal reduces the diffraction intensity by 50%, and a double layer by 90%, at 300 eV. At lower electron energies the depth of penetration is further reduced.

The effects involved in the diffraction of low-energy electrons are considerably more complicated than the predictions of the scattering theory.[22] Most investigators have reported a number of "anomalous" beams in addition to the diffraction beams that are accounted for by the surface and volume conditions. The anomalous beams are observed at both normal and grazing incidence of the primary beam, and have still not been accounted for.

In earlier papers [2,3,9,23-25] most of the anomalous beams were attributed to contamination of the investigated surfaces. When crystals are heated close to their melting point in a high vacuum these beams are considerably attenuated but do not disappear entirely. Ion bombardment completely removes impurities in most cases, and in some instances the diffraction pattern is produced only by the lattice of the crystal surface.

2. Cleaning of surfaces. The procedure for obtaining atomically clean surfaces to be investigated by low-energy electron diffraction is outlined in [6]. The first step is outgassing for 50—100 hours at a high temperature (Table I).

The outgassing process is terminated when a stable pressure of 10^{-8} mm is established around the heated sample. After being cooled the sample is cleaned by argon-ion bombardment lasting a few minutes. Following an anneal at 500°C the cleaned surface is checked by examining a diffraction pattern.

*As a result of refraction the wavelength in a crystal is shorter than in a vacuum.

Table I. Conditions for cleaning of different crystals

Crystal	Outgassing temperature, ° C	Total duration of ion bombardment
Germanium	700—800	0.5—1.0 hr
Silicon	800—900	30 min
Titanium	800—1000	—
Nickel	800—1100	3.0 hr
Copper	900	—
Tungsten	1100—1600	—

Annealing following the ion bombardment is absolutely necessary because the diffraction pattern disappears after the bombardment and is restored only subsequently to the anneal. The procedure of ion cleaning followed by annealing is usually repeated several times. The total duration of the bombardment is 0.5—3 hr, depending on the crystal (Table I). Ion bombardment without preliminary outgassing does not produce the desired result. A correctly cleaned surface remains atomically clean 1—30 days if stored in a 10^{-9}—10^{-10} mm vacuum.

The (001) face of a titanium crystal and the (100) face of a nickel crystal cleaned by ion bombardment yielded diffraction patterns agreeing with the corresponding x-ray patterns.[28] Such agreement of the patterns is not always observed following ion cleaning. For example, the surface structures of germanium and silicon differed from those indicated by x rays. For this reason the possible sources of impurities during the cleaning process in the diffraction tube were studied.[6,26] The composition of residual gases was monitored by connecting the apparatus to a mass spectrometer. It was found that tungsten heaters in the cleaning compartment desorb nitrogen in an amount not exceeding 0.1 monolayer in the case of closest atomic packing. Oxygen from these heaters is not desorbed as a gas but in the form of tungsten oxides up to 2% monolayer. The total amount of other gases was 0.2% monolayer.

In order to determine the effect produced by a molybdenum crystal-holder the sample was separated from the holder by a layer of graphite, which led to the appearance of CO but did not change the previously observed diffraction pattern. It is therefore reasonable to conclude that the material of the crystal-holder is not a source of impurities. Gases are desorbed from the heaters into the diffraction tube in too negligible amounts to be impurity sources. Another suspected source was the diffusion of impurity atoms (dissolved gases, carbon etc.) from the interior of the sample crystal to its surface. A special investigation[6] showed that if diffusion does occur the concentration of foreign atoms on the surface must be too small to affect the diffraction pattern.

Impurities introduced during the cleaning process are therefore too insignificant to account for the structure of the (100) face of germanium in the (110) azimuth. It must be assumed that the surface layers contain atoms displaced from their normal sites in the bulk crystal. The observed diffraction pattern with half-integral reflection orders can be explained[6,28] by assuming that atoms are displaced through a distance of many atomic diameters in a direction perpendicular to the (110) azimuth.

A more complicated structure has been found in the (100) and (111) faces of a silicon crystal.[27] In addition to the ordinary spacing, additional structures are observed with spacings depending on the conditions of argon-ion bombardment and the subsequent heat treatment (Table II).

A proposed structure of the (111) face of silicon is shown in Fig. 8. The additional surface structures, represented here by solid circles, may possibly be much more complex, since several different lattices can be constructed with the given periodicities; Fig. 8 shows only the simplest versions.

In [29] changes of the surface structure were not observed following annealing or quenching. However, the conditions of surface cleaning differed here from those given in Table II. This provides additional proof that the structure of silicon surface layers depends strongly on the cleaning process.

3. Structure of residual gas layers on metal surfaces. Investigations performed with low-energy electrons show that atomically pure metal surfaces cannot be achieved by outgassing alone at a high temperature even in a 10^{-9} mm vacuum. Gas layers were still found to remain even when a surface was heated to the evaporation temperature and was partially evaporated.[16] It appears at the present time that atomically pure metal surfaces free of any gas layers can only be produced by argon-ion bombardment.

We shall now consider the structures of some of the

Table II. Structures of (100) and (111) silicon surfaces depending on cleaning and heat treatment[41]

Surface	Treatment	Structure
A (111)	Annealed at 650° C for a few hr after heating at 1000° C for a few min following ion bombardment at 150 to 500 eV	A spacing 7 times that of silicon and the same lattice orientation as in silicon
B (111)	Radiation quenched from 1000° C after ion bombardment at 500 eV	A spacing $(19)^{1/2}$ times that of silicon and rotated 23.5° from the silicon lattice
C (111)	Radiation quenched from 1000° C after ion bombardment at 150 eV	Reflections from normal silicon lattice very strong; additional sublattice probably similar to A or B
D (100)	Annealed at 650° C for a few hr subsequent to heating at 1000° C for a few min or subsequent to argon-ion bombardment	Half-spaced surface lattice in azimuths having even sums of indices [similar to results for (100) germanium surface]
E (100)	Radiation quenched from 1000° C	Spacings about 8% greater than that of normal silicon plus the sublattice in D

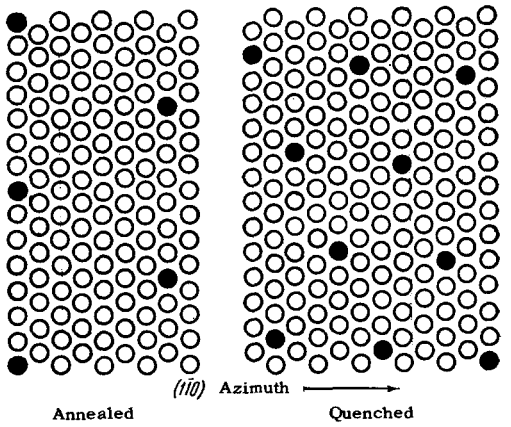

FIG. 8. (111) surface of silicon cleaned by argon-ion bombardment. Two large-spaced structures (indicated by solid circles) were obtained following annealing and quenching. Open circles indicate normal positions of silicon atoms.

most frequently encountered gas layers on metal surfaces. In the initial stages of outgassing at temperatures up to 700°C the (100) face of copper crystals revealed no regular diffraction pattern.[12,30] This indicates the presence of a very thick gas film having a disordered structure. Following outgassing at 900°C the (100) surface exhibited a monolayer having a square lattice and the same spacing as in the (100) face of copper. Outgassing above 900°C (with partial evaporation of the copper) changed the structure of the gaseous monolayer, which was now face-centered having spacing half that of the (100) copper face. Similar results have been obtained for nickel,[12,30] which exhibits the first structure at 600—1000°C and the second structure at 1100°C. Gas layers with similar structures were observed on almost all the investigated metals prior to any ion bombardment.

An investigation of hydrogen layers[31] determined the pressure region in which the aforementioned gaseous structures are formed. The second structure is formed at pressures < 0.5 mm and the first structure in relatively thick layers is formed at 2 mm. Figure 9 shows examples of diffraction patterns from gas layers.

It must be remembered that for gas layers with one-half the metal lattice spacing the refractive index is unity, while for layers with unchanged spacing the index is greater than unity. This difference of the refractive index for different structures has still not been accounted for.

4. Dependence of diffraction patterns on experimental conditions and geometry. Temperature effect. Low-energy electron diffraction resembles x-ray diffraction with regard to this effect. The intensity reduction of diffracted beams as a function of temperature is given by

$$I_m = I_0 \exp\left[-q\left(V+\frac{\varphi}{\sin^2\Theta}\right)(T-T_0)\right], \qquad (6)$$

where V is the accelerating potential, φ is the inner

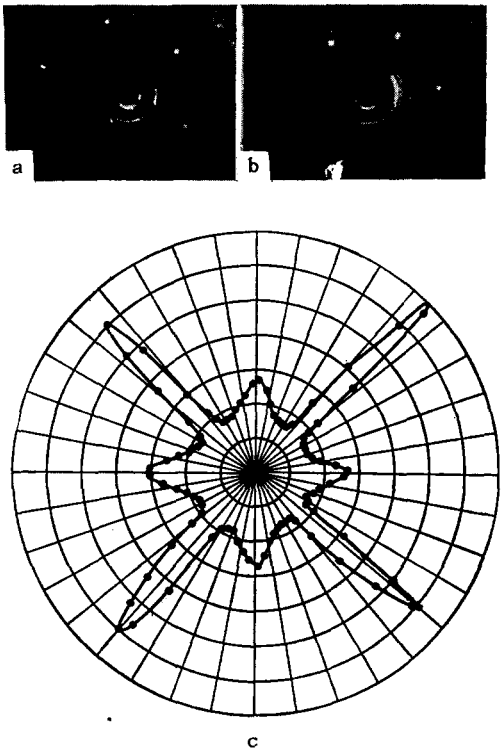

FIG. 9. a) Diffraction pattern of (111) nickel surface; b) diffraction pattern of oxygen layer on (111) nickel surface; c) diffraction pattern of gas layer on (100) copper surface. The beams are of half-integral orders with symmetry in the (111) azimuth. Collector angle 48°; primary-beam energy 45.5 eV.

potential of the lattice, and q is a constant for all beams. The complete theory of the temperature effect is given in [5].

Diffraction satellites. An investigation of low-energy electron diffraction from a (100) copper surface[16] revealed weaker maxima on the higher-potential sides of the main maxima (Fig. 10). The refractive index was unity for the main beams and greater than unity for the satellites.

More intense satellites have been observed in diffraction by silver than by copper. We have still no rigorous explanation for the appearance of satellites and for their intensities.[16,31]

It is of considerable interest to compare the diffraction patterns of silver and gold, which are known to possess identical structures and almost identical spacings.[32] The differences observed in the diffraction patterns suggest that the diffracting system is not a single lattice but consists of many sublattices comprising 5—10 rows of atoms and similar but not identical orientations. The author of [32] attributes the differences between the diffraction patterns of gold and silver exclusively to the atomic properties of these elements.

Influence of geometry on diffraction intensities. The investigation of crystal surfaces at normal incidence of the primary beam is extremely sensitive to very small deviations from perpendicularity, which affect

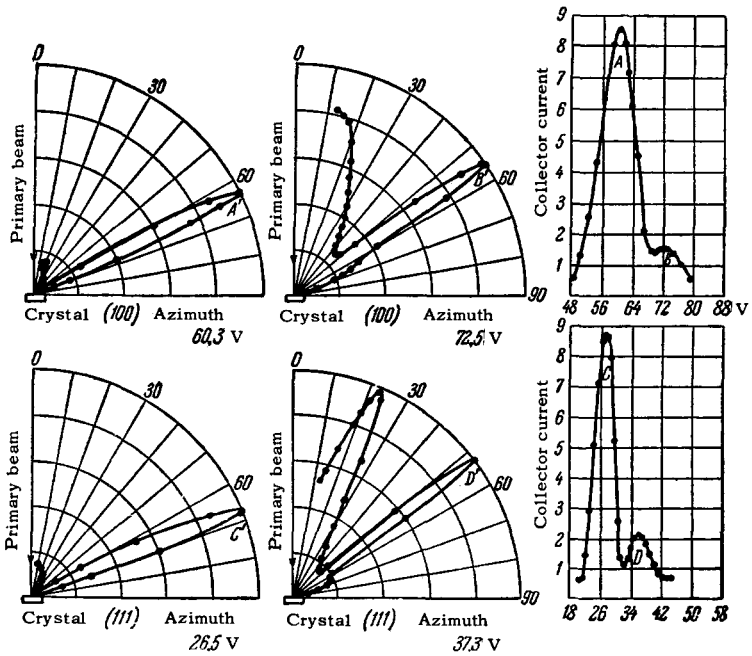

FIG. 10. Diffraction curves for a (100) copper surface. The maxima B and D are the satellites of the main beams A and C, respectively. The colatitude curves A′B′C′D′ correspond to the maxima ABCD.

mainly the diffraction beam intensities. The shapes of diffraction peaks are also changed, and their positions are shifted slightly.

Figure 11 shows diffraction beams from a (100) copper surface which were registered for normal incidence as well as for slight departures from perpendicularity.

The experimental procedure requires not only careful positioning of samples but subsequent checking of the adjustment in the course of the experiment. For this purpose sin Θ is plotted as a function of $\lambda = (150/V)^{1/2}$. Evidence of correct sample positioning is obtained when the experimental points are well fitted by straight lines (Fig. 12).

The intensities and shapes of diffraction beams are greatly affected by the geometry of the sample crystal,

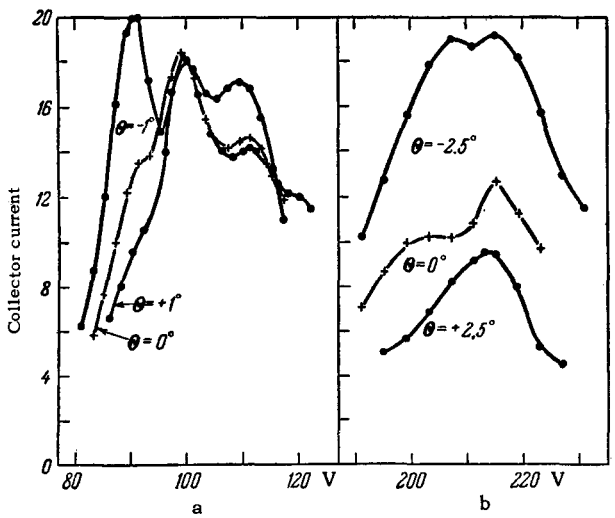

FIG. 11. Diffraction maxima from a (100) copper surface for normal and off-normal primary-beam incidence. Both a and b are second-order reflections in the (111) azimuth.

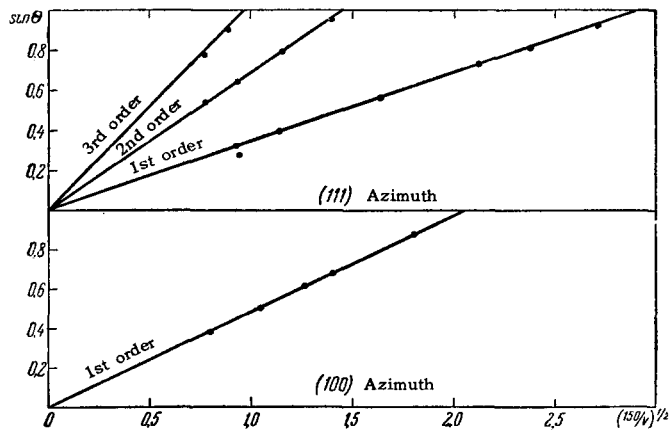

FIG. 12. Plot of sin Θ against $\lambda = (150/V)^{1/2}$ for different azimuths and normal incidence on a (100) silver surface.

[33] i.e., by the type of surface and by its direction in the crystal. For example, when a silver crystal is cut so that its (100) plane is parallel to its surface and the primary beam is directed at normal incidence to this (100) plane, reflection from the (210) plane must also appear (Fig. 13). However, (210) reflection will also be observed when the primary beam is normal to the (110) plane.* Diffraction beams for these different orientations are represented in Fig. 14a. The differences of the shapes cannot be attributed only to the properties of the (100) and (110) planes, but can also be associated with different refractive indices. Similar considerations can be applied to the (520) plane and the associated diffraction curves in Fig. 14b.

*Crystals having the given orientations can be obtained by etching in nitric acid.[34]

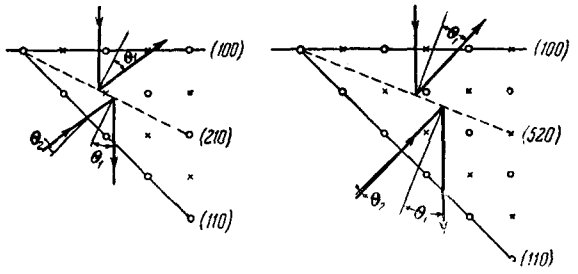

FIG. 13. Section of a silver lattice normal to the [001] direction. The (100), (210), (110), and (520) planes are normal to the plane of the figure.

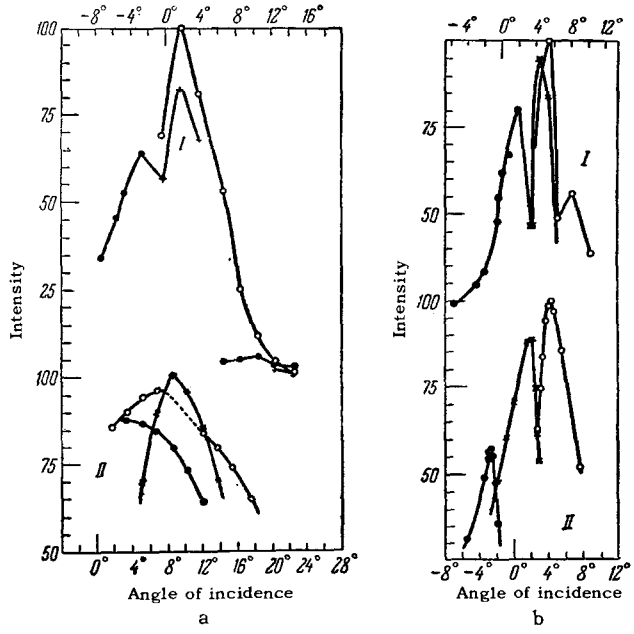

FIG. 14. Diffraction beams for different angles of incidence on a silver crystal. a) I – first-order reflections from the (210) plane for normal incidence on the (100) surface; II – first-order reflections from the (210) plane for normal incidence on the (110) surface. b) I – first-order reflections from the (520) plane for normal incidence on the (100) surface; II – first-order reflections from the (520) plane for normal incidence on the (110) surface.

Beams of different intensities and shapes can also result from incidence on opposite sides of the normal to a given plane. This effect was detected in the study of diffraction from the (111) plane of a face-centered cubic crystal. Asymmetric beams were registered in the (111) and (100) azimuths for 41° incidence; a doublet and a singlet were obtained, respectively.

Resolving power of the crystal and apparatus. The resolving power in low-energy electron diffraction has been discussed only in [9]. The resolving power of the apparatus depends on the size of the collector opening and on its distance from the crystal. For the diffraction tube described in [9] it was found that the actual resolving power is higher than would be expected from the corresponding dimensions (diameter of collector opening 1 mm and distance to crystal 19 mm). The effective diameter of the collector opening is found to be smaller than its geometric diameter because of the retarding potential applied to the boxes comprising the collector.

The background-to-maximum current ratio depends mainly on the design of the diffraction chamber. The potential range in which diffraction beams are observed depends both on the beam intensity and on the accelerating potential. For example, in the case of copper a 26.5-eV beam can be registered at 23.5 eV and at 30.5 eV, giving $\Delta\lambda/\lambda = 0.125$. At higher potentials diffraction beams appear in narrower wavelength intervals. As the accelerating potential is varied the change of the diffraction angle is such that the product $V^{1/2} \sin \Theta$ remains approximately constant.

III. SOME APPLICATIONS OF LOW-ENERGY ELECTRON DIFFRACTION

1. Determination of the inner potential of a crystal lattice. The determination of the inner potential has been illustrated above for tungsten. A diffraction tube without a magnetic field [9] was used to obtain the inner potential for the (100) copper surface. In this case, as previously, the inner potential was the difference between the computed beam potential and its experimental value for a suitably selected refractive index. It was found that as the computed potential increases from a low value the inner potential grows up to a saturation value (Fig. 15). The increase of the inner potential for low calculated potentials of diffraction beams is associated with a strong gradient of the inner potential at a depth of 1 or 2 atomic layers on the surface.

The dependence of the inner potential on the state and method of cleaning (111) and (100) silicon surfaces has been investigated in [41].

2. Adsorption of gas layers. The study of gas adsorption by atomically clean metal surfaces using low-energy electrons has revealed the initial stages of this process. Other techniques for the investigation of adsorption do not obtain information on the structure of gas monolayers. Therefore different hypotheses have

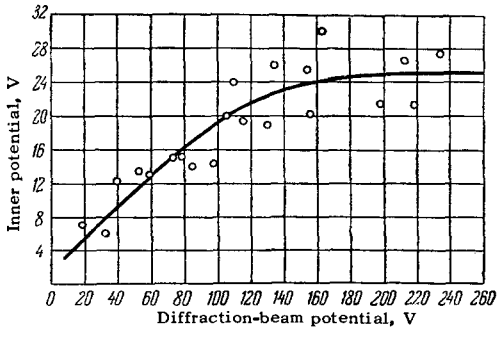

FIG. 15. The inner potential of a (100) copper face as a function of the calculated diffraction-beam potential.

been advanced regarding the initial stages of gas adsorption on metals.[35]

Low-energy electron diffraction permits the study of the gas adsorption process while a surface is still not completely covered with a monolayer. The adsorption of oxygen on an atomically clean (100) nickel face was studied in [36]. At room temperature a face-centered monolayer is formed with spacing half that of the underlying nickel. The monolayer covers the surface completely following an exposure (oxygen-pressure × time) of 2×10^{-6} mm-min. With further increase of the exposure, i.e., with growth of the adsorbed layer, the ordered structure of the gas layer disappears. After an exposure of 10^{-5} mm-min at room temperature the formation of nickel oxide is observed. Upon heating to 250—300°C the adsorbed oxygen layer and the oxide disappear.

When the crystal surface is contaminated with carbon (having the same structure as the oxygen monolayer) the oxide is formed over the impurity. This shows that nickel atoms diffuse through an impurity layer to the adsorbed oxygen layer.

The adsorption of oxygen and nitrogen at room temperature, and of oxygen at the temperature of an ice-acetone mixture, on a (100) face has been investigated in [12,37]; the relation between the gas pressure and the diffraction current is shown in Fig. 16. The curves

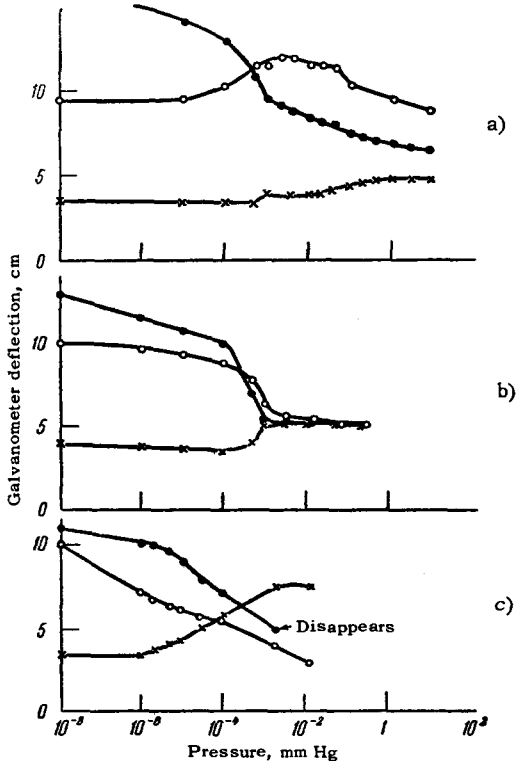

FIG. 16. Diffraction-beam current versus gas pressure when oxygen and nitrogen are adsorbed on a (100) copper face at different temperatures. a) Nitrogen adsorption at room temperature; b) nitrogen adsorption at the temperature of an ice-acetone mixture; c) oxygen adsorption at room temperature.

pertaining to nitrogen adsorption approach a single limit, which is attained for high pressures at room temperature. The initially high intensity in Fig. 16a is evidence of lattice perfection in this pressure range. Oxygen adsorption differs in character from nitrogen adsorption at the same temperatures. When oxygen or nitrogen is adsorbed on a (0001) titanium face the gas layer has the same hexagonal symmetry and lattice constant as the titanium crystal.[37] Adsorbed oxygen layers strongly affect the properties of germanium crystals, reducing their photoconductivity and lifetime, and increasing the work function.[38,39]

In one of the most recent investigations [27] a technique was developed for determining the fraction of a surface covered by an adsorbed gas as well as a method of calculating the probability that a molecule will stick to an adsorbing surface, using low-energy electron diffraction data. The fractional coverage can be evaluated from the diffraction-beam currents as a function of the exposure, subject to the following necessary assumptions:

1. Scattering from the covered portion of the surface is coherent with scattering from the uncovered portion. This can occur only if the adsorbed gas is distributed uniformly on the surface.

2. Beam amplitudes from the uncovered portion are proportional to the uncovered area. In this case $A_1 = A_0(1-\Theta)$, where A_1 is the scattering amplitude from the uncovered portion, A_0 is the scattering amplitude from the clean surface, and Θ is the determined fractional coverage (for complete coverage $\Theta = 1$).

3. Beam amplitudes from the covered portion of the surface can be represented as the sum of two amplitudes—from a clean surface (modified by added gas layers) and from ordered gas layers.

4. The proposed formula for the scattering amplitude from a clean surface is $A_2 = aA_0\Theta e^{i\alpha}$, where a is a constant and α is the phase difference of scattering from the two portions. The diffraction amplitude from the ordered portion of the gas layer is represented by $A_3 = b\Theta e^{i\rho}$. The total scattering amplitude is then the sum

$$A = A_0 - Be^{i\gamma}\Theta, \tag{7}$$

where

$$Be^{i\gamma} = A_0 - A_0 ae^{i\alpha} - be^{i\varphi}, \tag{8}$$

and the intensity is

$$I = A_0^2 - A_0 B[\cos\gamma]\Theta + B^2\Theta^2. \tag{9}$$

If it is assumed that the beam current is proportional to I, the foregoing equation can be solved for Θ; since $I = I_0$ for $\Theta = 0$ and $I = I_1$ for $\Theta = 1$, we have

$$\Theta = \frac{I_0^{1/2}\cos\gamma - (I_0\cos^2\gamma - I_0 + I)^{1/2}}{I_0^{1/2}\cos\gamma - (I_0\cos^2\gamma - I_0 + I_1)^{1/2}}, \tag{10}$$

where γ is an experimentally determined parameter. However, we have

$$1 \geqslant \cos^2\gamma \geqslant \frac{I_0 - I}{I_0} \qquad (11)$$

for the smallest observed values of I (usually I_1). Thus we have

$$\frac{I_0^{1/2} - I^{1/2}}{I_0^{1/2} - I_1^{1/2}} \geqslant \Theta \geqslant 1 - \frac{(I - I_1)^{1/2}}{(I_0 - I_1)^{1/2}}. \qquad (12)$$

The best results are obtained when upon successive additions of oxygen (or of another gas) the diffraction beam disappears. In this case $I_1 = 0$ and $\Theta = 1 - (I/I_0)^{1/2}$. The sticking probability of a gas molecule is defined as the ratio of the adsorption rate to the sticking rate.[40]

In order to calculate the sticking probability we must determine the number of adsorbed molecules per unit surface at $\Theta = 1$. For an exposure of 1 mm-min to oxygen we obtain 4.3×10^{22} atoms/cm^2 at 300°K. If N_S atoms/cm^2 are adsorbed when $\Theta = 1$ the sticking probability is

$$S = \frac{N_s}{4.3 \cdot 10^{22}} \frac{d\Theta}{d\left(\int p\,dt\right)}, \qquad (13)$$

where $\int p\,dt$ is the exposure in mm Hg-min.

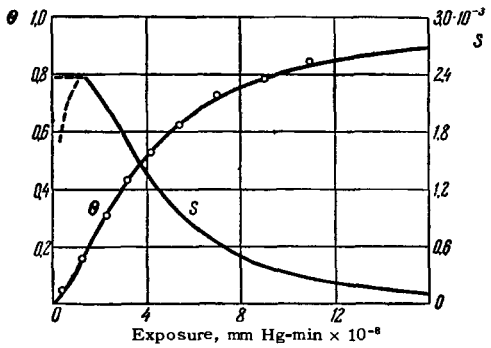

FIG. 17. Fractional coverage Θ and sticking probability S for a (100) surface of germanium as functions of exposure to oxygen at 300° K.

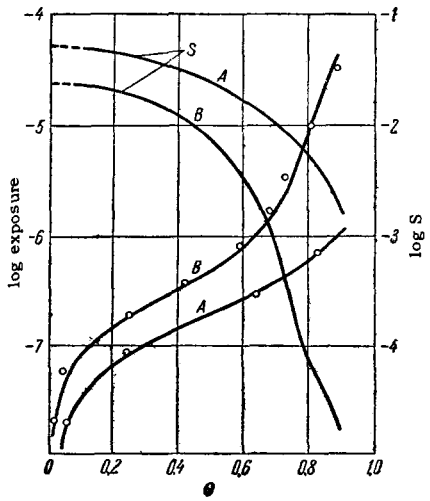

FIG. 18. Exposure and sticking probability S for a (100) silicon surface as functions of fractional coverage for oxygen adsorption at 300° K. Curves A and B are for the annealed and quenched surface, respectively.

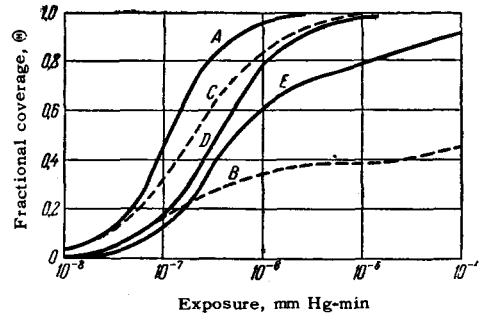

FIG. 19. Fractional coverage for oxygen adsorption on silicon crystal faces. The letters on the curves correspond to the letters in Table II for different conditions of surface treatment.

Figures 17 and 18 show the properties of oxygen adsorption on (100) germanium and silicon faces. The oxygen adsorption rate is proportional to pressure up to 10^{-6} mm.

Data showing the effect of surface treatment on the fractional coverage by oxygen are shown in Fig. 19.[41] The surface state is shown to have an extremely strong influence on the adsorption rate.

CONCLUSION

The experimental techniques now employed in low-energy electron diffraction permit the resolution of specific problems regarding the structures and properties of solid surfaces.[42]

This diffraction method has been used very effectively recently only to investigate gas adsorption and to determine the inner potentials of crystal lattices. At the same time this has led to the very important discovery that gas monolayers have an ordered structure. Application of the method to other phenomena such as the photoeffect and electron emission will undoubtedly lead to new qualitative results. The lack of a theory of low-energy electron diffraction still prevents any quantitative treatment of the experimental data. Therefore the diffraction patterns must be interpreted with extreme caution.

[1] V. M. Luk'yanovich, Élektronnaya mikroskopiya v fiziko-khimicheskikh issledovanniyakh (Electron Microscopy in Physical and Chemical Investigations) AN SSSR, Moscow, 1960.

[2] C. J. Davisson and L. H. Germer, Phys. Rev. **30**, 705 (1927).

[3] C. J. Davisson and L. H. Germer, Proc. Natl. Acad. Sci. U.S. **14**, 317 (1928).

[4] C. J. Davisson and L. H. Germer, Proc. Natl. Acad. Sci. U. S. **14**, 619 (1928).

[5] Z. G. Pinsker, Difraktsiya élektronov (Electron Diffraction), AN SSSR, Moscow, 1949.

[6] Farnsworth, Schlier, George, and Burger, J. Appl. Phys. **29**, 1150 (1958).

[7] H. E. Farnsworth, Rev. Sci. Instr. **21**, 102 (1950).

[8] H. E. Farnsworth, Rev. Sci. Instr. **15**, 290 (1927).

[9] H. E. Farnsworth, Phys. Rev. **34**, 679 (1929).
[10] W. T. Sproull, Rev. Sci. Instr. **4**, 193 (1933).
[11] H. E. Farnsworth, Phys. Rev. **44**, 417 (1933).
[12] R. E. Schlier and H. E. Farnsworth, J. Appl. Phys. **25**, 1333 (1954).
[13] H. D. Hagstrum, Rev. Sci. Instr. **24**, 1122 (1953).
[14] Scheibner, Germer, and Hartman, Rev. Sci. Instr. **31**, 112 (1960).
[15] R. T. Bayard and D. Alpert, Rev. Sci. Instr. **21**, 571 (1950).
[16] H. E. Farnsworth, Phys. Rev. **40**, 684 (1932).
[17] W. Ehrenberg, Phil. Mag. **18**, 878 (1934).
[18] J. A. Becker and C. D. Hartman, J. Phys. Chem. **57**, 153 (1953).
[19] H. E. Farnsworth, Rev. Sci. Instr. **31**, 795 (1960).
[20] W. T. Sproull, Phys. Rev. **43**, 516 (1933).
[21] H. E. Farnsworth, Phys. Rev. **49**, 605 (1936).
[22] H. A. Bethe, Ann. Physik **87**, 55 (1928); P. M. Morse, Phys. Rev. **35**, 1310 (1930); M. von Laue, Phys. Rev. **37**, 53 (1931); R. de L. Kronig and W. G. Penney, Proc. Roy. Soc. (London) **A130**, 499 (1931); E. L. Hill, Phys. Rev. **37**, 785 (1931); P. M. Morse and W. P. Allis, Phys. Rev. **44**, 269 (1933).
[23] E. Rupp, Ann. Physik **5**, 453 (1930).
[24] H. E. Farnsworth, Phys. Rev. **36**, 1799 (1930); **35**, 1131 (1930).
[25] W. Boas and E. Rupp, Ann. Physik **7**, 983 (1930).
[26] Farnsworth, Schlier, George, and Burger, J. Appl. Phys. **26**, 252 (1955).
[27] R. E. Schlier and H. E. Farnsworth, J. Chem. Phys. **30**, 917 (1959).
[28] R. E. Schlier and H. E. Farnsworth, in Semiconductor Surface Physics, U. of Pennsylvania Press, Philadelphia, 1957, p. 3; Farnsworth, Schlier, and Burger, Phys. Rev. **98**, 250 (1955).
[29] H. E. Farnsworth and R. E. Schlier, Bull. Am. Phys. Soc. **3**, 30 (1958).
[30] R. E. Schlier, Phys. Rev. **90**, 351 (1953).
[31] H. E. Farnsworth, Phys. Rev. **35**, 1131 (1930).
[32] H. E. Farnsworth, Phys. Rev. **43**, 900 (1933); **42**, 588 (1932).
[33] H. E. Farnsworth, Phys. Rev. **43**, 778 (1933); **49**, 598 (1936).
[34] H. E. Farnsworth, Phys. Rev. **40**, 684 (1932).
[35] Shishakov, Andreeva, and Andrushchenko, Stroenie i mekhanizm obrazovaniya okisnykh plenok na metallakh (Structure and Mechanism of Oxide Film Formation on Metals), AN SSSR, Moscow, 1959, p. 177.
[36] R. E. Schlier and H. E. Farnsworth, in Advances in Catalysis, **9**, Academic Press, Inc., New York, 1957, p. 434.
[37] R. E. Schlier and H. E. Farnsworth, Phys. Rev. **90**, 351 (1953); George, Farnsworth, and Schlier, J. Chem. Phys. **31**, 89 (1959).
[38] H. H. Madden and H. E. Farnsworth, Bull. Am. Phys. Soc. **1**, 53 (1956).
[39] J. A. Dillon, Bull. Am. Phys. Soc. **1**, 53 (1956).
[40] M. W. Roberts, J. Roy. Inst. Chem. **84**, 275 (1960).
[41] Farnsworth, Schlier, and Dillon, J. Phys. Chem. Solids **8**, 116 (1959).
[42] D. A. Gorodetskiĭ and A. M. Kornev, Abstracts of 10th Conference on Cathode Electronics, Tashkent, November 30, 1961.

Translated by I. Emin